



HAL
open science

Gate-Controlled Skyrmion Chirality

Charles-Elie Fillion, Johanna Fischer, Raj Kumar, Aymen Fassatoui, Stefania Pizzini, Laurent Ranno, Djoudi Ourdani, Mohamed Belmeguenai, Yves Roussigné, Salim-Mourad Chérif, et al.

► **To cite this version:**

Charles-Elie Fillion, Johanna Fischer, Raj Kumar, Aymen Fassatoui, Stefania Pizzini, et al.. Gate-Controlled Skyrmion Chirality. 2022. hal-03617498v1

HAL Id: hal-03617498

<https://hal.science/hal-03617498v1>

Preprint submitted on 23 Mar 2022 (v1), last revised 12 Apr 2022 (v2)

HAL is a multi-disciplinary open access archive for the deposit and dissemination of scientific research documents, whether they are published or not. The documents may come from teaching and research institutions in France or abroad, or from public or private research centers.

L'archive ouverte pluridisciplinaire **HAL**, est destinée au dépôt et à la diffusion de documents scientifiques de niveau recherche, publiés ou non, émanant des établissements d'enseignement et de recherche français ou étrangers, des laboratoires publics ou privés.

Gate-Controlled Skyrmion Chirality

Charles-Elie Fillion,¹ Johanna Fischer,¹ Raj Kumar,¹ Aymen Fassatoui,² Stefania Pizzini,² Laurent Ranno,² Djoudi Ourdani,³ Mohamed Belmeguenai,³ Yves Roussigné,³ Salim-Mourad Chérif,³ Stéphane Auffret,¹ Isabelle Joumard,¹ Olivier Boulle,¹ Gilles Gaudin,¹ Liliana Buda-Prejbeanu,¹ Claire Baraduc,¹ and Hélène Béa¹

¹*Univ. Grenoble Alpes, CEA, CNRS,*

Grenoble INP, IRIG-Spintec, Grenoble, France*

²*Univ. Grenoble Alpes, CNRS, Néel Institute, Grenoble, France*

³*Laboratoire des Sciences des Procédés et des Matériaux (LSPM), Villetaneuse, France*

(Dated: March 22, 2022)

Abstract

Magnetic skyrmions are localized chiral spin textures, which offer great promise to store and process information at the nanoscale. In the presence of asymmetric exchange interactions, their chirality, which governs their dynamics, is generally considered as an intrinsic parameter set during the sample deposition. In this work, we experimentally demonstrate that this key parameter can be controlled by a gate voltage. We observed that the current-induced skyrmion motion can be reversed by the application of a gate voltage. This local and dynamical reversal of the skyrmion chirality is due to a sign inversion of the interfacial Dzyaloshinskii-Moriya interaction that we attribute to ionic migration of oxygen under gate voltage. Micromagnetic simulations show that the chirality reversal is a continuous transformation, in which the skyrmion is conserved. This gate-controlled chirality provides a local and dynamical degree of freedom, yielding new functionalities to skyrmion-based logic devices.

PACS numbers:

* Institute of Engineering Univ. Grenoble Alpes

12 Magnetic skyrmions are spin-swirling, topologically nontrivial spin textures that hold
 13 promise for next-generation spintronic devices¹⁻⁵. Their nanometric size and efficient ma-
 14 nipulation by electric current⁶ would enable high storage density and fast computational
 15 operations. In thin multilayered ferromagnetic films, skyrmions are characterized by circu-
 16 lar, homochiral Néel domain walls (DWs) which are stabilized by interfacial Dzyaloshinskii-
 17 Moriya interaction (iDMI)^{7,8}. The sign of the iDMI constant D sets the preferred chirality
 18 of the Néel DW⁹. With our conventions, Néel DW adopts a right-handed or clockwise (CW)
 19 chirality for $D < 0$ and a left-handed or counterclockwise (CCW) chirality for $D > 0$.
 20 Besides, chirality plays a key role in the DW dynamics driven by spin-orbit torques⁹⁻¹². In
 21 heavy-metal/ferromagnet/metal-oxide (HM/FM/MO_x) trilayers, a charge current flowing in
 22 the HM layer generates a transverse spin current due to the spin Hall effect whose angular
 23 momentum is transferred to the FM magnetization¹³. The resulting spin-orbit torque moves
 24 DWs and skyrmions in a direction that depends on their chirality and on the sign of the
 25 spin Hall angle (SHA). For instance, a HM underlayer with negative SHA, such as Ta^{14,15},
 26 induces a motion of CW DWs along the current density whereas CCW DWs move along the
 27 electron flow¹⁵.
 28 It is generally considered that iDMI is an intrinsic parameter set during the sample depo-
 29 sition. The effective iDMI in HM/FM/MO_x trilayers is the sum of the contributions origi-
 30 nating from the two FM interfaces and may be adjusted by varying the FM thickness^{16,17},
 31 removing the metal-oxide¹⁸, changing the type of HM^{19,20} or the oxidation state at the
 32 FM/MO_x interface^{21,22}. Recently, it has been shown that tuning the oxidation state of the
 33 FM/MO_x interface can invert the iDMI sign²³. However, these techniques to control iDMI
 34 and thus DW chirality are limited to material engineering. Controlling iDMI using an ex-
 35 ternal excitation thus opens a novel degree of freedom to efficiently manipulate chiral spin
 36 textures such as magnetic skyrmions²¹.
 37 In particular, gate voltage control of interfacial magnetic properties²⁴⁻²⁶ offers a promising,
 38 low power and versatile technique to achieve both a local and dynamical control of iDMI.
 39 It is well-established that a gate voltage can modify the charge distribution and tune the
 40 oxidation state at the FM/MO_x interface, both mechanisms leading to changes in interfacial
 41 magnetic anisotropy²⁷. The strongest effect associated with non-volatility has been explained
 42 as driven by O²⁻ ionic migration towards the interface or away from it, depending on the
 43 voltage polarity²⁸⁻³⁰. Such ionic migration is already exploited as a mechanism for resistive

44 switching in anionic metal oxide memristor devices³¹. This tuning of interfacial magnetic
45 anisotropy has allowed to control with a gate the creation and annihilation of skyrmions³²⁻³⁵.
46 Furthermore, it was demonstrated that the iDMI amplitude is reversibly tunable with a gate
47 voltage^{26,36,37} due to its interfacial nature. The possibility to electrically reverse the sign of
48 the iDMI would provide a versatile and reversible control of skyrmion chirality, which could
49 considerably improve their all-electrical, low power manipulation.

50 In this article, we demonstrate experimentally that a gate voltage induces a local and dynam-
51 ical reversal of skyrmion chirality in Ta/FeCoB/TaO_x trilayer. Moreover, we show a similar
52 effect on chiral DWs in a labyrinthine magnetic state, confirming our findings on magnetic
53 skyrmions. We show that regardless of the initial DW chirality, which is controlled by the
54 initial oxidation level at the FeCoB/TaO_x interface, a gate voltage with appropriate polarity
55 is able to switch chirality back and forth in a persistent way. This reversal is attributed to
56 ionic migration, and thus oxidation or reduction of the FeCoB/TaO_x interface, by the gate
57 voltage, which results in the inversion of iDMI sign. Finally, using micromagnetic simula-
58 tions we show that an adiabatic chirality reversal of a nanometer size skyrmion is possible in
59 Co-based sample. The internal structure of the DW evolves continuously from one chirality
60 to the other without skyrmion annihilation when iDMI is vanishing.

61 **Skyrmion Chirality Reversal with Gate Voltage**

62 A schematic representation of the Ta(3)/FeCoB(1.2)/TaO_x(0.85-1) trilayer (nominal thick-
63 nesses in nm), with 20 nm ZrO₂ oxide and transparent Indium Tin Oxide (ITO) electrode
64 (See *Methods*), is shown in Fig. 1a. The oxidation step after the top-Ta wedge deposition
65 induces an oxidation gradient at the top interface (see Fig. 1b). This gradient induces a
66 sign crossover of iDMI, as deduced by an inversion of the current-induced motion (CIM)
67 of magnetic skyrmions and chiral DWs and confirmed by direct iDMI measurements via
68 Brillouin Light Scattering (BLS) (see Supplementary, section I). The use of polar-Magneto-
69 Optical Kerr-Effect (p-MOKE) microscope through transparent electrodes allows us to di-
70 rectly observe the CIM and its inversion during or after the application of a gate voltage
71 (See *Methods*).

72 In the area close to the iDMI sign crossover (star location in Fig. 1b), an external out of
73 plane magnetic field $\mu_0 H_{ext} \simeq 80 \mu\text{T}$ stabilizes magnetic bubbles of $\simeq 1 \mu\text{m}$ diameter (white

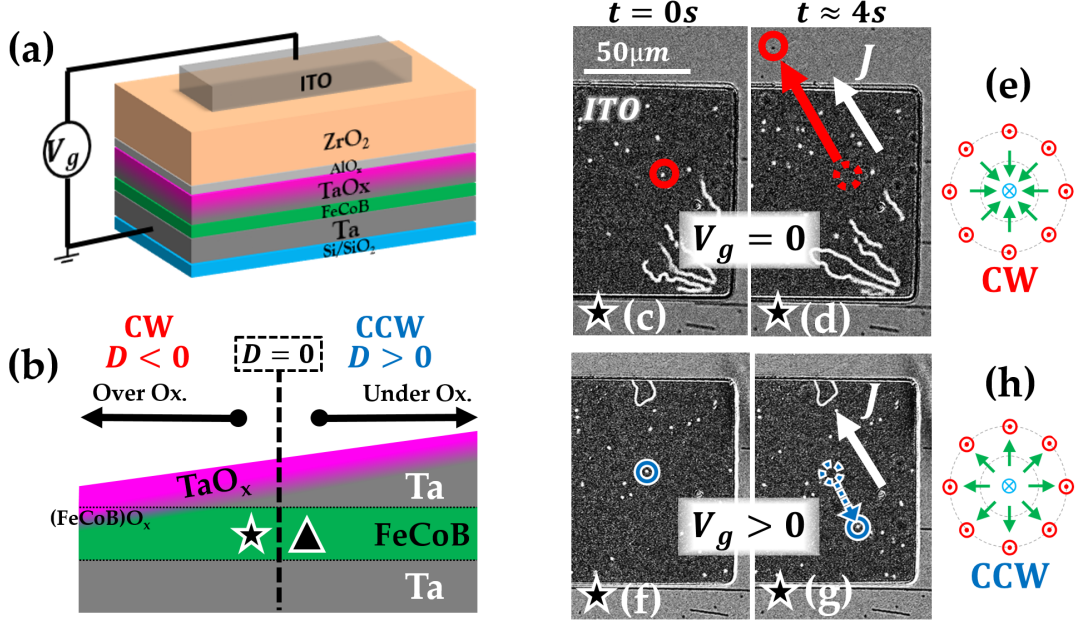


FIG. 1: **Skyrmion chirality switch** - (a) Schematic representation of the Ta/FeCoB/TaO_x trilayer with additional ZrO₂ oxide and transparent ITO electrode for gate voltage application. (b) Schematic cross section of the sample: the top-Ta wedge induces an oxidation gradient at the top interface, leading to a iDMI sign crossover for slightly underoxidized TaO_x. (c-d) CIM monitored during 4 s under p-MOKE microscope at the star location shown on (b) for zero gate voltage and (f-g) for $V_g = +3.5\text{V}$, applied on ITO (the dark rectangular region). The in-plane current density ($J \simeq 5 \times 10^9 \text{ A.m}^{-2}$) is represented by the white arrow and the out of plane magnetic field is $\mu_0 H_{ext} \simeq 80 \mu\text{T}$. (c-d) In the initial state, skyrmions move in the direction of the current (encircled skyrmion moving along the red arrow), indicating CW chirality ($D < 0$), schematically represented in (e). (f-g) Under the positive gate voltage, an inversion of the skyrmion motion occurs (encircled skyrmion moving along the blue arrow), indicating a CCW chirality ($D > 0$), as represented in (h).

74 dots under ITO in Fig. 1(c,d,f,g)). When a current is applied, magnetic bubbles drift in the
 75 same direction confirming their skyrmionic nature and their homochirality. We call them
 76 skyrmions in the following, since they share the same topology³⁸. Due to the low injected
 77 current density ($J \simeq 5 \times 10^9 \text{ A.m}^{-2}$, see Supplementary section II), some skyrmions remain
 78 motionless as they are probably pinned by defects.

79 In the initial state ($V_g = 0$), the mobile skyrmions move along the current direction (speed
80 $v_{0V} = 13.5 \pm 2 \mu\text{m.s}^{-1}$ at $J \simeq 5 \times 10^9 \text{ A.m}^{-2}$) which is expected for a Néel DW with a
81 CW chirality (see red circles in Fig.1c-d, and Supplementary Video SV1). It is noteworthy
82 that the effect of the thickness gradient on the skyrmion motion is negligible, indicating
83 that current is the driving force (see Supplementary, section III). Besides, skyrmion Hall
84 effect is expected to be negligible due to the small velocities in this regime of low current
85 densities³⁹⁻⁴¹. Furthermore, the continuous motion of skyrmions when crossing the edges
86 of the electrode shows that the magnetic configuration is the same below and around the
87 electrode.

88 Skyrmion CIM is then measured while applying a positive gate voltage on the electrode
89 (Fig. 1f-g). We observe a progressive change: skyrmion speed first decreases, then the
90 motion direction inverts, typically after 90 s, and speed further increases and saturates. The
91 CIM is now along the electron flow with $v_{+3.5V} = 3.2 \pm 2 \mu\text{m.s}^{-1}$ at $J \simeq 5 \times 10^9 \text{ A.m}^{-2}$ (see
92 Supplementary, section IV, and Video SV2). Such inversion of motion is a signature of a
93 transition from CW to CCW chirality, induced by an inversion of iDMI sign with voltages
94 compatible with applications. As expected, this CIM reversal is observed only below the ITO
95 electrode, where the FeCoB/TaO_x interface properties are modified by the gate voltage. This
96 effect is reversible: switching the gate voltage to zero allows recovering the as-grown CW
97 skyrmion chirality, on the time scale of several minutes. Moreover, the chirality inversion
98 is reproducible: skyrmions in Fig. 1a have previously undergone several chirality reversals.
99 A more detailed analysis of skyrmions trajectories of Fig. 1(c,d,f,g) and their inversion can
100 be found in Supplementary, section IV, as well as the results of an experiment over a larger
101 number of skyrmions, allowing extensive statistics.

102 Our experimental observations show that the gate voltage produces the same effect as a
103 displacement along the Ta wedge from the region with $D < 0$ (star in Fig. 1b) to the
104 region with $D > 0$ (triangle in Fig. 1b): starting from the region where skyrmions have
105 CW chirality (as represented in Fig. 1e), a positive gate-voltage leads to a reversal to
106 CCW chirality (as represented in Fig. 1h). Thus, a positive gate-voltage induces interfacial
107 magnetic properties similar to those of a less oxidized interface. We may interpret this
108 result either as a charge effect or as a migration of oxygen ions away from the interface. The
109 former should produce an immediate effect whereas the latter is expected to be slower and
110 possibly persistent. Since our measurements show that the reversal of the skyrmion motion

111 occurs with a certain latency, we propose that the driving mechanism is ion migration. The
112 positive gate voltage acts as a local reduction of the FeCoB/TaO_x interface that triggers
113 the chirality reversal. Moreover, the recovery of the as-grown chirality when switching-off
114 the gate voltage ($V_g = 0$) is consistent with the spontaneous re-oxidation of the FM/MO_x
115 interface observed in similar materials with an equivalent timescale⁴².

116 Persistent and Reversible Control of Chirality with Gate Voltage

117 Hereafter, we explore the chirality reversal process on labyrinthine domains (see Fig. 2)
118 obtained by decreasing the external magnetic field to 30 μ T in a region of the sample similar
119 to the one of Fig. 1(c,d,f,g). This magnetic configuration is more robust than skyrmions to
120 small changes of magnetic parameters and magnetic field¹¹. Here, we focus on the persistent
121 effect of gate voltage on DW chirality. Thus, the current injection experiments, to probe
122 the chirality, were performed after turning off the gate voltage.

123 Fig. 2a shows the initial nearly demagnetized state with labyrinthine domains. The pattern
124 of the labyrinthine domains is identical and continuous below and around the electrode. In
125 the initial state, before gate voltage application, the DWs move in the same direction as
126 the current, which is an indication of their CW chirality (see Fig. 2a, Supplementary Video
127 SV3). After the application of a 90 s positive gate voltage pulse ($V_g = 3$ V), the CIM of the
128 DWs below the electrode is reversed (see Fig. 2b, Supplementary Video SV4), indicating a
129 CCW chirality, which is due to an inversion of iDMI sign. This result is similar to the one
130 obtained for skyrmions, except that the domain wall chirality is now probed at remanence,
131 *ie.* $\simeq 5$ s after the gate voltage has been set to zero.

132 We further observed that a 90 s negative gate voltage pulse ($V_g = -2$ V) restores the initial
133 CW chirality (Fig. 2c, Supplementary Video SV5). A subsequent 90 s positive gate voltage
134 pulse ($V_g = 3$ V) once again switches towards CCW chirality (Fig. 2d, Supplementary Video
135 SV6). Thus, chirality can be reversibly controlled by gate voltage and in a persistent way.
136 It is reversed from CW to CCW (resp. from CCW to CW) with a positive (resp. negative)
137 gate voltage, which we attribute to reduction (resp. oxidation) of the FeCoB/TaO_x interface
138 (see Fig. 2g). Moreover, this local and dynamical control of the chirality is realized with
139 voltages compatible with applications ($|V_g| \simeq 2 - 3$ V).

140 The reversed CCW DWs of Fig. 2d recover their initial CW chirality after about two hours

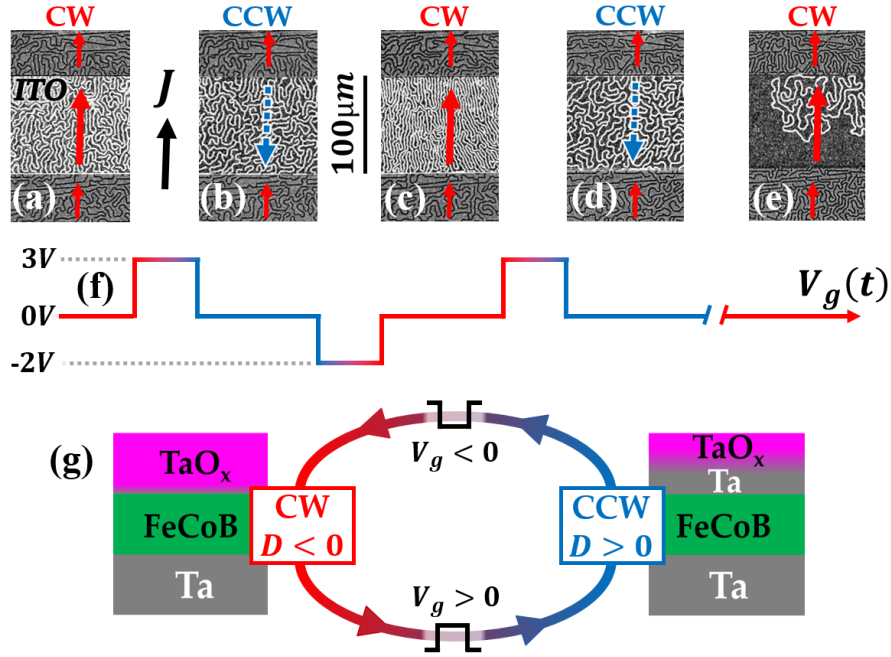


FIG. 2: **Persistent and reversible chirality switch** - In the region close to iDMI sign inversion (star in Fig. 1b), the current density J (black arrow) induces a motion of DWs (red/blue arrows for a motion along/opposite to the current density), as observed by p-MOKE microscopy after switching off the gate voltage. (a-e) observation of DW motion under zero gate voltage and $\mu_0 H_{ext} \simeq 30 \mu\text{T}$, after sequential 90s-long voltage pulses. (f) Schematic representation of the applied voltage as a function of time. Initially (a) DW have CW chirality; after a positive gate voltage pulse (b), chirality is reversed to CCW under the ITO electrode; after a negative gate voltage pulse (c), CW chirality is recovered; after a positive gate voltage pulse (d), chirality has switched again to CCW; (e) after waiting ~ 2 hours with zero gate voltage applied, the initial CW chirality is recovered. (g) Schematics of the effect of gate voltage pulses on interface oxidation, DW chirality and iDMI.

141 (Fig. 2e, Supplementary Video SV7), which is longer than for skyrmions (see previous
 142 section). In this experiment, negative voltages were applied to the FM/MO_x interface (ox-
 143 idation of the interface), which is known to induce irreversibility^{21,30} and that may be at
 144 the origin of a slower recovery of magnetic properties. We suggest that the positive gate
 145 voltage drives oxygen ions from their equilibrium position into a metastable less oxidized
 146 state, in which they remain after the gate voltage has been turned off. The existence of such

147 a metastable state has been theoretically demonstrated at Fe/MgO interface, in the opposite
148 case, ie. when interfacial oxygen is migrated towards the first Fe layer⁴³. The slow recovery
149 of the initial state, also reported in other studies^{44,45}, corresponds to a return to equilibrium.
150 The time scale of this process is consistent with our hypothesis of ion migration, which is
151 known to occur in TaO_x and ZrO_x³¹.

152 Finally, we have observed that chirality control can be achieved either starting from a neg-
153 ative iDMI (zone indicated by the star in Fig. 1b, see Fig. 2) or from a positive iDMI
154 (zone indicated by the triangle in Fig. 1b, see Supplementary, section V), by applying a
155 gate voltage of appropriate polarity, as schematically represented in Fig 2g.

156 **Stability of skyrmions under chirality reversal: analytical model and micromagnetic** 157 **simulations**

158 The observed inversion of the skyrmion CIM under the application of a gate voltage is the
159 signature of a transition between CW and CCW Néel skyrmions, which results from a iDMI
160 sign inversion. In principle, this transition is possible without unravelling the spin texture
161 since CW Néel, CCW Néel and the expected intermediate Bloch skyrmion at zero iDMI
162 share the same topology. However, even if this transformation is topologically allowed, it
163 may affect the energetic stability of the skyrmion, in particular the stability of the Bloch
164 skyrmion at zero iDMI. In the absence of stabilization by iDMI energy in thin films, only
165 dipolar energy and out of plane external magnetic field may stabilize Bloch skyrmions⁴⁶.
166 To evaluate the stability of skyrmions during the application of a gate voltage, we have
167 considered an analytical model describing the energy difference between an isolated skyrmion
168 bubble and the uniform magnetic state³³ (See *Methods*). The magnetic parameters used in
169 this analytical model and their variation under positive gate voltage are those extracted
170 from experimental measurements (see Supplementary section VI).

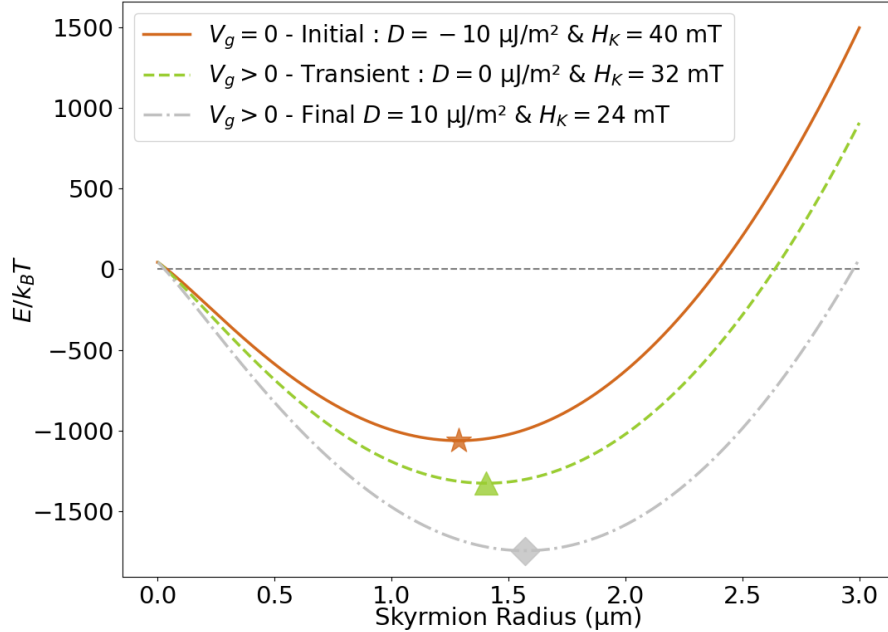


FIG. 3: **Analytical model³³: stability of skyrmions in FeCoB during iDMI inversion induced by the gate voltage** - Analytical calculation of energy difference (in units of $k_B T_{300K}$) between skyrmion and uniform state for FeCoB as a function of skyrmion diameter. Solid orange, dashed green and dash-dotted gray lines correspond respectively to negative, zero and positive iDMI, associated to a progressive anisotropy variation under the gate voltage, as experimentally measured. Due to the small iDMI value in FeCoB, the slight change of equilibrium diameter (depicted by symbols) is mostly due to the anisotropy variation.

171 The model predicts that for both non-zero and zero iDMI, a skyrmion is stable for di-
 172 ameters around $1.5 \mu\text{m}$, close to the experimental values (see Fig. 3). Only a slight change
 173 of equilibrium diameter is expected, mostly due to the anisotropy variations under gate
 174 voltage, since our iDMI values, relatively small ($|D| \simeq 10 \mu\text{J}/\text{m}^2$ interpolated from BLS
 175 measurements, see Supplementary section VI), contribute little to the total energy of the
 176 skyrmion. According to the model, it should be possible to reverse the chirality of a single
 177 skyrmion without annihilating it.

178 To better understand the mechanism of the chirality reversal, we carried out micromagnetic
 179 simulations⁴⁷ (See *Methods*). These enable investigating the chirality reversal mechanism

180 at small dimensions inaccessible with the experimental setup of our study (Kerr microscope
 181 resolution $\simeq 0.5 \mu\text{m}$). The magnetic parameters used in this simulation (Co-based magnetic
 182 parameters⁴¹, see *Methods*) lead to sub-micrometer size skyrmions, which are more relevant
 183 for applications. These small skyrmions cannot be described by the previous analytical
 184 calculations since their DW cannot be considered as infinitely thin with respect to skyrmion
 185 diameter. By contrast, they are more adapted to micromagnetic simulations as they require
 186 a reasonable number of cells. For small skyrmions, the iDMI contribution to the total energy
 187 is larger and we may thus wonder if their stability might be affected. The simulations were
 188 performed for iDMI value in the range $[-0.5; 0.5] \text{ mJ/m}^2$. For each iDMI value, a magnetic
 189 skyrmion is stabilized, in particular for $D = 0$ where a Bloch skyrmion is stable (see Fig.
 190 4a-c). We note that such a variation of iDMI of $\Delta D = 1 \text{ mJ/m}^2$ by a gate voltage requests
 191 an electric field of $E = 1 \text{ V/nm}$, which is below the breakdown electric field in similar
 192 ZrO_x -based sample⁴². This would require a iDMI variation efficiency under electric field
 193 $\beta_{iDMI} = \Delta D/E$ of 1000 fJ/(Vm) , which is a proper order of magnitude for ionic effects³⁷ or
 194 in the case of ultrathin ferromagnets²⁶.

195 In the center of the DW, the angle ξ between the in-plane magnetic moments and the radial
 196 direction, usually named helicity, evolves gradually from $|\xi| = 0$ at $D = -0.5 \text{ mJ/m}^2$ (CW
 197 Néel, see Fig. 4a) to $|\xi| = \pi$ at $D = 0.5 \text{ mJ/m}^2$ (CCW Néel, see Fig. 4c) via a $|\xi| = \frac{\pi}{2}$
 198 Bloch skyrmion state at $D = 0$ (see Fig. 4b). The radius variation between Néel and Bloch
 199 skyrmion (from 165 nm to 22 nm , see fig 4f) is much larger than in the analytical model
 200 prediction for FeCoB (see Fig. 3). This may be explained by a larger decrease of domain
 201 wall energy thanks to iDMI for the case of the Co-based sample (micromagnetic simulation).
 202 In these zero temperature simulations, the evolution of ξ with iDMI (see Fig. 4d) presents
 203 a hysteretic behavior around $|D| = 0.35 \text{ mJ/m}^2$. It corresponds to the beginning of the
 204 coherent rotation of the moments in the DW, selecting one of the two degenerated states
 205 leading to a CW or CCW Bloch skyrmion at $D = 0$ (see Supplementary, section VII).

206 Discussion

207 Our observations of chirality reversal are due to gate voltage effect on iDMI. The effec-
 208 tive iDMI originates from the two FeCoB interfaces in Ta/FeCoB/TaO_x. At the bottom
 209 Ta/FeCoB interface, the Fert-Levy mechanism^{48,49} is at the origin of a small, negligible

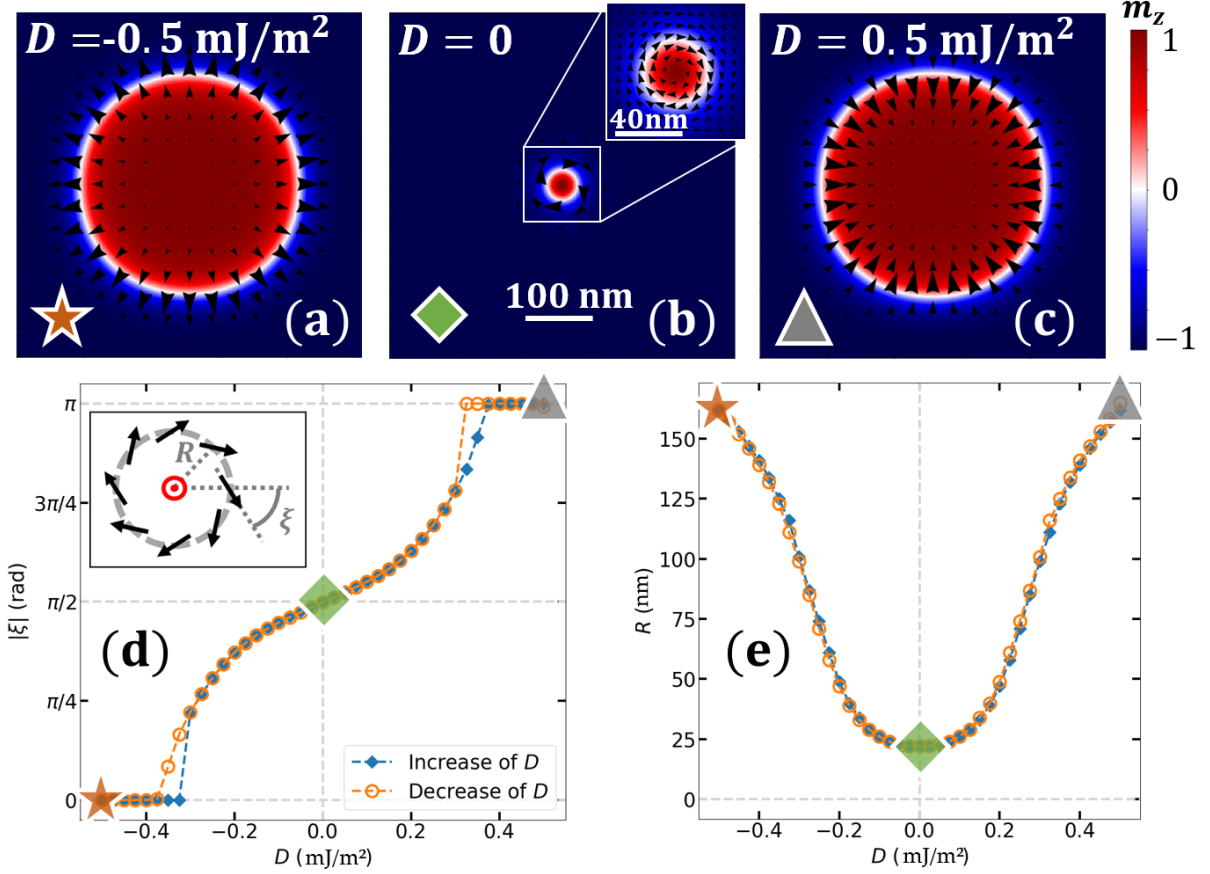


FIG. 4: **Micromagnetic simulations of chirality switch** - Simulated stable states show a gradual transition between (a) CW Néel skyrmion at $D = -0.5 \text{ mJ/m}^2$ and (c) CCW Néel skyrmion at $D = 0.5 \text{ mJ/m}^2$ via (b) a stable Bloch skyrmion state at $D = 0$.

(d) Angle ξ between the in-plane magnetic moments and the radial direction of the magnetic moments at the domain-wall center and (e) radius of the skyrmion as a function of the iDMI value. The helicity and radius of the skyrmion corresponding to a-c images are shown respectively in (d) and (e) by the star, square and triangle symbols.

210 negative iDMI contribution^{19,50} (typically -0.03 mJ/m^2). The origin of iDMI for the top
 211 FeCoB/TaO_x interface depends on oxidation state: (i) an underoxidized FeCoB/Ta top in-
 212 terface leads to a dominant Fert-Levy contribution to iDMI, with opposite sign with respect
 213 to the iDMI from the bottom interface and with larger magnitude due to intermixing⁵⁰.
 214 This leads to a positive effective iDMI. (ii) By contrast, by gradually oxidizing this inter-
 215 face, the interfacial electric field at the origin of Rashba effect⁵¹ is modified, resulting in a

216 contribution to iDMI¹⁸ found to be negative in this system^{37,59}. Towards the more oxidized
217 region, this Rashba contribution becomes dominant and determines the negative sign of
218 the effective iDMI. Our experiments are done in the region where the contributions from
219 the two interfaces almost cancel each other. Then, iDMI values are very small ($|D| \simeq 10$
220 $\mu\text{J}/\text{m}^2$) and should result in hybrid Bloch-Néel domain walls, so called Dzyaloshinskii walls
221 (see supplementary section VII, Fig S9(d,f,h,j)). However, the observed CIM aligned with
222 the current density is the expected behaviour of Néel DWs. In any case, an inversion of the
223 iDMI sign leads to the inversion of the Néel component of the DW, which similarly leads to
224 an inversion of the CIM direction.

225 It has been demonstrated that the perpendicular magnetic anisotropy and the iDMI have
226 common origins, and are thus both sensitive to voltage¹⁸ and oxidation²². Then, similarly
227 to voltage control of magnetic anisotropy²⁷ (VCMA), an applied gate voltage can produce
228 instantaneous reversible charge effects on iDMI³⁷ or persistent ones linked to ionic migration
229 (see supplementary of reference³⁷). In the case of charge effects, the short screening length
230 in metals (shorter than the FeCoB film thickness) would mainly modify charge distribution
231 at the interface with the oxide. The addition of the applied electric field to the Rashba-field
232 could reverse the total interfacial electric field, inducing an inversion of iDMI sign.

233 Nevertheless, we have shown that the effect of the gate voltage produces a similar effect as
234 a displacement along the oxidation gradient. This is consistent with ion migration affecting
235 the top FeCoB/TaO_x interface. This ion migration induced by gate voltage may lead to
236 a transition between negative Rashba and positive Fert-Levy contribution to iDMI. As we
237 observed persistent effect on the time scale of minutes, we propose that ionic migration is the
238 dominant mechanism observed in our study. Oxygen ions are most probably the migrating
239 ions, as they are the mobile species in ZrO₂. However, we cannot exclude the possibility of
240 cation or proton migration⁴⁴.

241 Since iDMI may also be tuned by charge effects³⁷ that occur as sub-nanosecond time scale⁵²,
242 we may envision an ultra fast switch of skyrmion chirality through a transient Bloch state.
243 Furthermore, contrary to a current polarity inversion, which would invert similarly the
244 motion direction of all skyrmions in the track, a gate voltage would provide a simple and
245 local method to individually control skyrmions. Notably, their individual motion tuning
246 can be fully exploited in race logic where information is stored in propagation time^{53,54}.
247 Eventually, due to the persistency of the effect, we may envision their use in artificial neural

248 networks based on cross bar geometries⁵⁵ with multiple gates to dynamically and reversibly
249 control the exact path of each input skyrmion. Besides, skyrmion motion along a track
250 could be stopped by a Néel to Bloch transition using a gate voltage. This would enable an
251 alternative realization of a skyrmion transistor hitherto proposed using VCMA^{56,57}. Finally,
252 this chirality switch offers a new degree of freedom which could be used in reversible and
253 programmable logic gates.

254 **Conclusion**

255 We have demonstrated a gate-voltage induced reversal of skyrmion chirality in
256 Ta/FeCoB/TaO_x through the inversion of their current induced motion direction. Besides,
257 we also observed a local, persistent and reversible chirality reversal of labyrinthine chiral
258 domain walls by gate voltage. These reversals are due to an inversion of the iDMI sign and
259 explained by the gate-controlled modification of the oxidation state at the ferromagnet/oxide
260 interface. Micromagnetic simulations support the feasibility of a chirality reversal for sub-
261 micronic skyrmions without annihilation. Such local and dynamical degree of freedom at
262 the nanometer scale would lay the foundations for efficient and multifunctional architectures
263 involving magnetic skyrmions as information carriers.

264 **Methods**

265 **Sample preparation**

266 The base sample consists in a Ta(3)/FeCoB(1.1-1.3)/Ta(0.85-1) (nominal thicknesses in
267 nm) crossed double wedge trilayer grown by magnetron sputtering on a thermally oxidized
268 Si/SiO₂ wafer⁵⁸. The top Ta wedge was further oxidized in a treatment chamber (oxygen
269 pressure 150 mbar for 10 s) thus leading to an oxidation gradient at the top interface (see
270 Fig. 1a). In order to protect from further oxidation, a 0.5nm layer of Al was deposited and
271 subsequently oxidized at air when taking the sample out of the sputtering machine. The final
272 stack thus consists in a Ta(3)/FeCoB(1.1-1.3)/TaO_x(0.85-1)/AlO_x(0.5) (thicknesses in nm).
273 Then, the sample was annealed (225°C for 30min) and a 20nm-ZrO₂ oxide was deposited
274 by atomic layer deposition. This oxide layer acts as a dielectric and a ionic conductor. For
275 this study, we restricted ourselves to a constant ferromagnetic thickness ($t_{FeCoB} \simeq 1.2$ nm,

276 at which skyrmions are observed), thus simplifying the sample to a single top Ta wedge,
277 as shown in Fig. 1a. The wedge of FeCoB was only used in the determination of some
278 parameters (see Supplementary Section VI). Finally, 70nm transparent ITO electrodes were
279 patterned by laser lithography. The size of the electrodes is $100 \times 800 \mu\text{m}^2$.

280 Skyrmion observation, current-induced motion

281 The use of p-MOKE under transparent ITO electrodes allows probing the magnetization
282 configuration both under and around the electrodes. Differential imaging is used in order
283 to improve the contrast (the reference is the saturated magnetic state). Under ITO (resp.
284 around it), black (resp. grey) regions correspond to magnetization pointing up, and white
285 (resp. black) regions to magnetization pointing down. This variation of contrast might be
286 explained by anti-reflecting effect from the ITO electrodes.

287 The skyrmion or labyrinthine phase (resp. in Fig. 1 and 2) is obtained by applying a
288 constant perpendicular field ($\mu_0 H_{ext}$ of 80 and 30 μT respectively), after saturating the
289 magnetic state with a field of same polarity. Meanwhile, a current is injected in the trilayer
290 plane before applying any gate voltage in order to probe the initial chirality through the CIM
291 direction. Then, the current is turned off and at this point, the measurement is different
292 between skyrmions and labyrinthine domains.

293 For skyrmions, a gate voltage is continuously applied. During this time, chirality is regularly
294 probed (every $\simeq 20$ s) by injecting current during sufficient time for the CIM to be measured.
295 For labyrinthine domains, voltage pulses are applied on the gate and CIM is measured after
296 each pulse, *i.e.* when the voltage is turned off.

297 In differential imaging, mechanical drift can degrade the contrasts. To avoid it, the reference
298 is renewed before each CIM measurement (short pulse of large magnetic field at which a new
299 reference is taken). Finally, to illustrate the motion, a color-coded set of arrows indicates
300 the CIM direction in Fig.1 and 2.

301 Analytical Model and Micromagnetic simulations

302 The analytical model from ref³³ estimates the energy difference between an individual
303 skyrmion of radius R and the saturated magnetic state. One must notice that this model

304 is valid for $Q = \frac{K_u}{K_d} > 1$, where K_u is the uniaxial anisotropy and $K_d = \frac{1}{2}\mu_0 M_s^2$ is the shape
 305 anisotropy constant. In our case, we can extract from experimental parameters $Q = 1.02$,
 306 lying in the area of validity of the model. In this model, the energy difference between an
 307 individual skyrmion state and the saturated magnetization state is written as

$$\Delta E_{sb} = 2\pi R t \sigma_{DW} + 2\pi R^2 t \mu_0 M_S H_{ext} - \pi t^3 \mu_0 M_S^2 I(d)$$

308 where σ_{DW} is the domain wall energy (containing exchange, anisotropy and iDMI energy), t is
 309 the ferromagnetic layer thickness, R is the bubble radius, M_S is the saturation magnetization,
 310 $\mu_0 H_{ext}$ is the applied magnetic field and $I(d)$ is defined as

$$I(d) = -\frac{2}{3\pi} d \left[d^2 + (1 - d^2) \frac{E(u^2)}{u} - \frac{K(u^2)}{u} \right]$$

where $d = \frac{2R}{t}$, $u = \frac{d^2}{1+d^2}$ and $E(u)$, $K(u)$ are elliptic integral defined as

$$E(u) = \int_0^{\pi/2} \sqrt{1 - u \sin^2(\alpha)} d\alpha$$

$$K(u) = \int_0^{\pi/2} \frac{d\alpha}{\sqrt{1 - u \sin^2(\alpha)}}$$

311 The parameters used in the analytical model are the FeCoB experimental parameters. The
 312 saturation magnetization $M_s = 1.54 \pm 0.06$ MA/m was measured with Vibrating Sample
 313 Magnetometer (VSM). The uniaxial anisotropy field $\mu_0 H_K = 40$ mT, and its variation under
 314 the application of a positive gate voltage was measured through hard-axis hysteresis loop
 315 (see Supplementary section VI). The FeCoB thickness $t_{FM} = 0.57$ nm was used to take
 316 into account a magnetically dead layer, estimated with VSM measurements versus FeCoB
 317 nominal thickness. The exchange stiffness was fixed to $A_{ex} = 12$ pJ/m³⁷. Finally, an external
 318 magnetic field $\mu_0 H_{ext} = -750$ μ T was set in a direction opposite to the magnetization in
 319 the core of the skyrmion (destabilizing field).

320 Using micromagnetic simulations (Mumax3⁴⁷), we computed an isolated skyrmion in an
 321 infinite magnetic thin film by computing the demagnetizing field from an infinite sample
 322 acting on the simulation region (See Supplementary section VII).

323 The magnetic parameters for the simulation are $M_s = 1.42$ MA/m (magnetization), $t_{FM} =$
 324 0.9 nm (ferromagnetic thickness), $K_u = 1.27 \times 10^6$ J/m³ (uniaxial anisotropy), $\alpha = 0.37$
 325 (Gilbert damping) and $A_{ex} = 16$ pJ/m (exchange stiffness). In addition to the dipolar field,

326 an additional homogeneous magnetic field is set to $\mu_0 H_z = -6$ mT (destabilizing field). The
327 simulation region is a 512 nm square, with a mesh size $1 \text{ nm} \times 1 \text{ nm} \times 0.9 \text{ nm}$.
328 First, we checked for the stabilization of a skyrmion with a positive iDMI value $D = 0.5$
329 mJ/m² (Fig 4c). Then, we decreased the iDMI value from $D = 0.5$ mJ/m² to $D = -0.5$
330 mJ/m² by step of 5% and checked for the stabilization of skyrmion at each step. Finally,
331 with the same procedure, we increased the iDMI value back to the initial $D = 0.5$ mJ/m².
332 In this simulation, the magnetic moments in the center of the DW experience a CCW in-
333 plane rotation for both the decrease and the increase of iDMI. As a result, a CW Bloch
334 skyrmion is observed for the decrease (see Fig. 4b) and a CCW for the increase of iDMI
335 (See Supplementary, section VII).

336 **Data availability**

337 The datasets generated during and/or analysed during the current study are available
338 from the corresponding author on reasonable request.

339 **Code availability**

340 The custom codes used during the current study are available from the corresponding
341 author on reasonable request.

342 ¹ A. N. Bogdanov and D. A. Yablonskii, "Thermodynamically stable "vortices" in magnetically
343 ordered crystals. The mixed state of magnets," Zh. Eksp. Teor. Fiz., vol. 95, pp. 187–182, Jan.
344 1989.

345 ² W. Jiang, P. Upadhyaya, W. Zhang, G. Yu, M. B. Jungfleisch, F. Y. Fradin, J. E. Pearson,
346 Y. Tserkovnyak, K. L. Wang, O. Heinonen, S. G. E. te Velthuis, and A. Hoffmann, "Blowing
347 magnetic skyrmion bubbles," Science, vol. 349, pp. 283–286, July 2015.

348 ³ O. Boulle, J. Vogel, H. Yang, S. Pizzini, D. de Souza Chaves, A. Locatelli, T. O. Mendes,
349 A. Sala, L. D. Buda-Prejbeanu, O. Klein, M. Belmeguenai, Y. Roussigné, A. Stashkevich,
350 S. M. Chérif, L. Aballe, M. Foerster, M. Chshiev, S. Auffret, I. M. Miron, and G. Gaudin,

- 351 “Room-temperature chiral magnetic skyrmions in ultrathin magnetic nanostructures,” Nature
352 Nanotechnology, vol. 11, pp. 449–454, May 2016.
- 353 ⁴ A. Fert, N. Reyren, and V. Cros, “Advances in the physics of magnetic skyrmions and perspective
354 for technology,” Nature Review Materials, vol. 46, June 2017.
- 355 ⁵ X. Zhang, Y. Zhou, K. Mee Song, T.-E. Park, J. Xia, M. Ezawa, X. Liu, W. Zhao, G. Zhao, and
356 S. Woo, “Skyrmion-electronics: writing, deleting, reading and processing magnetic skyrmions
357 toward spintronic applications,” Journal of Physics: Condensed Matter, vol. 32, p. 143001, Apr.
358 2020.
- 359 ⁶ S. Woo, K. Litzius, B. Krueger, M.-Y. Im, L. Caretta, K. Richter, M. Mann, A. Krone, R. M.
360 Reeve, M. Weigand, P. Agrawal, I. Limesh, M.-A. Mawass, P. Fischer, M. Klaui, and G. S. D.
361 Beach, “Observation of room-temperature magnetic skyrmions and their current-driven dynamics
362 in ultrathin metallic ferromagnets,” Nature Materials, vol. 15, pp. 501–506, May 2016.
- 363 ⁷ I. E. Dzyaloshinskii, “Theory of helicoidal structures in antiferromagnets. i. nonmetals,” J. Exptl.
364 Theoret. Phys. (U.S.S.R.), vol. 46, no. 8, 1964.
- 365 ⁸ T. Moriya, “Anisotropic Superexchange Interaction and Weak Ferromagnetism,” Physical
366 Review, vol. 120, pp. 91–98, Oct. 1960.
- 367 ⁹ A. Thiaville, S. Rohart, E. Jué, V. Cros, and A. Fert, “Dynamics of Dzyaloshinskii domain walls
368 in ultrathin magnetic films,” EPL (Europhysics Letters), vol. 100, p. 57002, Dec. 2012.
- 369 ¹⁰ S. Woo, K. Litzius, B. Krueger, M.-Y. Im, L. Caretta, K. Richter, M. Mann, A. Krone, R. M.
370 Reeve, M. Weigand, P. Agrawal, I. Limesh, M.-A. Mawass, P. Fischer, M. Klaui, and G. S. D.
371 Beach, “Observation of room-temperature magnetic skyrmions and their current-driven dynamics
372 in ultrathin metallic ferromagnets,” Nature materials, vol. 15, pp. 501–506, Feb. 2016.
- 373 ¹¹ G. Yu, P. Upadhyaya, X. Li, W. Li, S. K. Kim, Y. Fan, K. L. Wong, Y. Tserkovnyak, P. K. Amiri,
374 and K. L. Wang, “Room-temperature creation and spin-orbit torque manipulation of skyrmions
375 in thin films with engineered asymmetry,” Nano Letters, vol. 16, pp. 1981–1988, Feb. 2016.
- 376 ¹² J. Iwasaki, M. Mochizuki, and N. Nagaosa, “Current-induced skyrmion dynamics in constricted
377 geometries,” Nature Nanotechnology, vol. 8, pp. 742–747, Sept. 2013.
- 378 ¹³ A. Hoffmann, “Spin Hall Effects in Metals,” IEEE Transactions on Magnetics, vol. 49, pp. 5172–
379 5193, Oct. 2013.
- 380 ¹⁴ L. Liu, C.-F. Pai, Y. Li, H. W. Tseng, D. C. Ralph, and R. A. Buhrman, “Spin-torque Switching
381 with the Giant Spin Hall Effect of Tantalum,” Science, vol. 336, pp. 555–558, May 2012.

- 382 ¹⁵ S. Emori, U. Bauer, S.-M. Ahn, E. Martinez, and G. S. D. Beach, “Current-driven dynamics of
383 chiral ferromagnetic domain walls,” Nature Materials, vol. 12, pp. 611–616, July 2013.
- 384 ¹⁶ R. Lo Conte, G. V. Karnad, E. Martinez, K. Lee, N.-H. Kim, D.-S. Han, J.-S. Kim, S. Prenzel,
385 T. Schulz, C.-Y. You, H. J. M. Swagten, and M. Klaui, “Ferromagnetic layer thickness depen-
386 dence of the Dzyaloshinskii-Moriya interaction and spin-orbit torques in Pt\Co\AlO_x,” AIP
387 Advances, vol. 7, p. 065317, June 2017.
- 388 ¹⁷ J. Cho, N.-H. Kim, S. Lee, J.-S. Kim, R. Lavrijsen, A. Solignac, Y. Yin, D.-S. Han, N. J. J.
389 van Hoof, H. J. M. Swagten, B. Koopmans, and C.-Y. You, “Thickness dependence of the
390 interfacial Dzyaloshinskii-Moriya interaction in inversion symmetry broken systems,” Nature
391 Communications, vol. 6, p. 7635, Nov. 2015.
- 392 ¹⁸ H. Yang, O. Boulle, V. Cros, A. Fert, and M. Chshiev, “Controlling Dzyaloshinskii-Moriya
393 Interaction via Chirality Dependent Atomic-Layer Stacking, Insulator Capping and Electric
394 Field,” Scientific Reports, vol. 8, p. 12356, Dec. 2018.
- 395 ¹⁹ X. Ma, G. Yu, C. Tang, X. Li, C. He, J. Shi, K. L. Wang, and X. Li, “Interfacial Dzyaloshinskii-
396 Moriya Interaction: Effect of 5 d Band Filling and Correlation with Spin Mixing Conductance,”
397 Physical Review Letters, vol. 120, p. 157204, Apr. 2018.
- 398 ²⁰ P. Jadaun, L. F. Register, and S. K. Banerjee, “The microscopic origin of DMI in magnetic
399 bilayers and prediction of giant DMI in new bilayers,” npj Computational Materials, vol. 6,
400 p. 88, Dec. 2020.
- 401 ²¹ L. Herrera Diez, Y. Liu, D. Gilbert, M. Belmeguenai, J. Vogel, S. Pizzini, E. Martinez, A. Lam-
402 perti, J. Mohammedi, A. Laborieux, Y. Roussigné, A. Grutter, E. Arenholtz, P. Quarterman,
403 B. Maranville, S. Ono, M. S. E. Hadri, R. Tolley, E. Fullerton, L. Sanchez-Tejerina, A. Stashke-
404 vich, S. Chérif, A. Kent, D. Querlioz, J. Langer, B. Ocker, and D. Ravelosona, “Nonvolatile
405 Ionic Modification of the Dzyaloshinskii-Moriya Interaction,” Physical Review Applied, vol. 12,
406 p. 034005, Sept. 2019.
- 407 ²² D. d. S. Chaves, F. Ajejas, V. Krizakova, J. Vogel, and S. Pizzini, “Dependence of Dzyaloshinskii-
408 Moriya interaction on the oxygen coverage in Pt/Co/MOx trilayers,” Physical Review B, vol. 99,
409 p. 144404, Apr. 2019. arXiv: 1708.08516.
- 410 ²³ M. Arora, J. M. Shaw, and H. T. Nembach, “Variation of sign and magnitude of the
411 Dzyaloshinskii-Moriya interaction of a ferromagnet with an oxide interface,” Physical Review
412 B, vol. 101, p. 054421, Feb. 2020.

- 413 ²⁴ M. Weisheit, S. Fahler, A. Marty, Y. Souche, C. Poinignon, and D. Givord, “Electric field-
414 induced modification of magnetism in thin-film ferromagnets,” Science Reports, vol. 315,
415 pp. 349–351, Feb. 2007.
- 416 ²⁵ W. G. Wang and C. L. Chien, “Voltage-induced switching in magnetic tunnel junctions with
417 perpendicular magnetic anisotropy,” Journal of Physics D: Applied Physics, vol. 46, p. 074004,
418 Jan. 2013.
- 419 ²⁶ M. Schott, L. Ranno, H. Béa, C. Baraduc, S. Auffret, and A. Bernand-Mantel, “Electric field
420 control of interfacial Dzyaloshinskii-Moriya interaction in Pt/Co/AlOx thin films,” Journal of
421 Magnetism and Magnetic Materials, vol. 520, p. 167122, Feb. 2021.
- 422 ²⁷ B. Dieny and M. Chshiev, “Perpendicular magnetic anisotropy at transition metal/oxide inter-
423 faces and applications,” Reviews of Modern Physics, vol. 89, p. 025008, June 2017.
- 424 ²⁸ C. Bi, Y. Liu, T. Newhouse-Illige, M. Xu, M. Rosales, J. Freeland, O. Mryasov, S. Zhang,
425 S. te Velthuis, and W. Wang, “Reversible Control of Co Magnetism by Voltage-Induced Oxida-
426 tion,” Physical Review Letters, vol. 113, p. 267202, Dec. 2014.
- 427 ²⁹ U. Bauer, L. Yao, A. J. Tan, P. Agrawal, S. Emori, H. L. Tuller, S. van Dijken, and G. S. D.
428 Beach, “Magneto-ionic control of interfacial magnetism,” Nature Materials, vol. 14, pp. 174–181,
429 Feb. 2015.
- 430 ³⁰ A. Fassatoui, J. P. Garcia, L. Ranno, J. Vogel, A. Bernand-Mantel, H. Béa, S. Pizzini, and
431 S. Pizzini, “Reversible and irreversible voltage manipulation of interfacial magnetic anisotropy
432 in Pt/Co/Oxide multilayers,” Phys. Rev. Applied, vol. 14, p. 064041, Dec. 2020.
- 433 ³¹ B. Mohammad, M. A. Jaoude, V. Kumar, D. M. Al Homouz, H. A. Nahla, M. Al-Qutayri, and
434 N. Christoforou, “State of the art of metal oxide memristor devices,” Nanotechnology Reviews,
435 vol. 5, Jan. 2016.
- 436 ³² Y. Nakatani, M. Hayashi, S. Kanai, S. Fukami, and H. Ohno, “Electric field control of Skyrmions
437 in magnetic nanodisks,” Applied Physics Letters, vol. 108, p. 152403, Apr. 2016.
- 438 ³³ M. Schott, A. Bernand-Mantel, L. Ranno, S. Pizzini, J. Vogel, H. Béa, C. Baraduc, S. Auffret,
439 G. Gaudin, and D. Givord, “The Skyrmion Switch: Turning Magnetic Skyrmion Bubbles on and
440 off with an Electric Field,” Nano Letters, vol. 17, pp. 3006–3012, May 2017.
- 441 ³⁴ C. Ma, X. Zhang, J. Xia, M. Ezawa, W. Jiang, T. Ono, S. N. Piramanayagam, A. Morisako,
442 Y. Zhou, and X. Liu, “Electric Field-Induced Creation and Directional Motion of Domain Walls
443 and Skyrmion Bubbles,” Nano Letters, vol. 19, pp. 353–361, Jan. 2019.

- 444 ³⁵ Y. Zhou, R. Mansell, and S. van Dijken, “Voltage control of skyrmions: Creation, annihilation,
445 and zero-magnetic field stabilization,” Applied Physics Letters, vol. 118, p. 172409, Apr. 2021.
- 446 ³⁶ K. Nawaoka, S. Miwa, Y. Shiota, N. Mizuochi, and Y. Suzuki, “Voltage induction of interfacial
447 Dzyaloshinskii-Moriya interaction in Au/Fe/MgO artificial multilayer,” Applied Physics Express,
448 vol. 8, p. 063004, June 2015.
- 449 ³⁷ T. Srivastava, M. Schott, R. Juge, V. Kryzakova, M. Belmeguenai, Y. Roussigné, A. Bernand-
450 Mantel, L. Ranno, S. Pizzini, S.-M. Chérif, A. Stashkevich, S. Auffret, O. Boulle, G. Gaudin,
451 M. Chshiev, C. Baraduc, and H. Béa, “Large-Voltage Tuning of Dzyaloshinskii-Moriya Interac-
452 tions: A Route toward Dynamic Control of Skyrmion Chirality,” Nano Letters, vol. 18, pp. 4871–
453 4877, Aug. 2018.
- 454 ³⁸ A. Bernand-Mantel, L. Camosi, A. Wartelle, N. Rougemaille, M. Darques, and L. Ranno, “The
455 skyrmion-bubble transition in a ferromagnetic thin film,” SciPost Physics, vol. 4, p. 027, May
456 2018.
- 457 ³⁹ C. Reichhardt and C. J. Olson Reichhardt, “Noise fluctuations and drive dependence of the
458 skyrmion Hall effect in disordered systems,” New Journal of Physics, vol. 18, p. 095005, Sept.
459 2016.
- 460 ⁴⁰ W. Jiang, X. Zhang, G. Yu, W. Zhang, X. Wang, M. Benjamin Jungfleisch, J. E. Pearson,
461 X. Cheng, O. Heinonen, K. L. Wang, Y. Zhou, A. Hoffmann, and S. G. E. te Velthuis, “Direct
462 observation of the skyrmion Hall effect,” Nature Physics, vol. 13, pp. 162–169, Feb. 2017.
- 463 ⁴¹ R. Juge, S.-G. Je, D. d. S. Chaves, L. D. Buda-Prejbeanu, J. Pena-Garcia, J. Nath, I. M. Miron,
464 K. G. Rana, L. Aballe, M. Foerster, F. Genuzio, T. O. Mentès, A. Locatelli, F. Maccherozzi,
465 S. S. Dhesi, M. Belmeguenai, Y. Roussigné, S. Auffret, S. Pizzini, G. Gaudin, J. Vogel, and
466 O. Boulle, “Current-Driven Skyrmion Dynamics and Drive-Dependent Skyrmion Hall Effect in
467 an Ultrathin Film,” Physical Review Applied, vol. 12, p. 044007, Oct. 2019.
- 468 ⁴² A. Fassatoui, L. Ranno, J. P. Garcia, C. Balan, J. Vogel, H. Bea, , and S. Pizzin, “Kinetics
469 of ion migration in the electric field-driven manipulation of magnetic anisotropy of pt/co/oxide
470 multilayers,” Small, vol. 17, p. 2102427, Sept. 2021.
- 471 ⁴³ F. Ibrahim, A. Hallal, B. Dieny, and M. Chshiev, “Establishing characteristic behavior of voltage
472 control of magnetic anisotropy by ionic migration,” Physical Review B, vol. 98, p. 214441, Dec.
473 2018.
- 474 ⁴⁴ A. J. Tan, M. Huang, C. O. Avci, F. Buettner, M. Mann, W. Hu, C. Mazzoli, S. Wilkins, H. L.

475 Tuller, and G. S. D. Beach, “Magneto-ionic control of magnetism using a solid-state proton
476 pump,” Nat. Mater., vol. 18, p. 35, Jan. 2019.

477 ⁴⁵ K.-Y. Lee, S. Jo, A. J. Tan, M. Huang, D. Choi, J. H. Park, H.-I. Ji, J.-W. Son, J. Chang, G. S. D.
478 Beach, and S. Woo, “Fast magneto-ionic switching of interface anisotropy using yttria-stabilized
479 zirconia gate oxide,” Nano Lett., vol. 20, p. 3435, May 2020.

480 ⁴⁶ A. Bernand-Mantel, C. B. Muratov, and T. M. Simon, “Unraveling the role of dipolar versus
481 dzyaloshinskii-moriya interactions in stabilizing compact magnetic skyrmions,” Phys. Rev. B,
482 vol. 101, p. 045416, Jan. 2020.

483 ⁴⁷ A. Vansteenkiste, J. Leliaert, M. Dvornik, M. Helsen, F. Garcia-Sanchez, and B. Van Waeyen-
484 berge, “The design and verification of MuMax3,” AIP Advances, vol. 4, p. 107133, Oct. 2014.

485 ⁴⁸ A. Fert and P. Levy, “Role of anisotropic exchange interactions in determining the properties of
486 spin-glasses,” Phys. Rev. Lett., vol. 44, p. 1538, Nov. 1980.

487 ⁴⁹ H. Yang, A. Thiaville, S. Rohart, A. Fert, and M. Chshiev, “Anatomy of Dzyaloshinskii-Moriya
488 Interaction at Co / Pt Interfaces,” Physical Review Letters, vol. 115, p. 267210, Dec. 2015.

489 ⁵⁰ L. H. Diez, M. Voto, A. Casiraghi, M. Belmeguenai, Y. Roussigné, G. Durin, A. Lamperti,
490 R. Mantovan, V. Sluka, V. Jeudy, Y. T. Liu, A. Stashkevich, S. M. Chérif, J. Langer, B. Ocker,
491 L. Lopez-Diaz, and D. Ravelosona, “Enhancement of the Dzyaloshinskii-Moriya interaction and
492 domain wall velocity through interface intermixing in Ta/CoFeB/MgO,” Physical Review B,
493 vol. 99, p. 054431, Feb. 2019.

494 ⁵¹ K.-W. Kim, H.-W. Lee, K.-J. Lee, and M. D. Stiles, “Chirality from Interfacial Spin-Orbit
495 Coupling Effects in Magnetic Bilayers,” Physical Review Letters, vol. 111, p. 216601, Nov. 2013.

496 ⁵² C. Grezes, F. Ebrahimi, J. G. Alzate1, X. Cai1, J. A. Katine, J. Langer, B. Ocker, P. K.
497 Amiri, , and K. L. Wang, “Ultra-low switching energy and scaling in electric-field-controlled
498 nanoscale magnetic tunnel junctions with high resistance-area product,” Appl. Phys. Lett.,
499 vol. 108, p. 012403, Jan. 2016.

500 ⁵³ V. H., M. N. SAKIB, S. GANGULY, M. STAN, M. W. DANIELS, A. MADHAVAN, M. D.
501 STILES, and A. W. GHOSH, “Temporal memory with magnetic racetracks,” IEEE Journal on
502 Exploratory Solid-State Computational Devices and Circuits, vol. 6, p. 107, Dec. 2020.

503 ⁵⁴ A. Madhavan, T. Sherwood, and D. Strukov, “Race logic: a hardware acceleration for dynamic
504 programming algorithms,” ACM SIGARCH Computer Architecture News, vol. 42, pp. 517–528,
505 June 2014.

- 506 ⁵⁵ Q. Xia and J. J. Yang, “Memristive crossbar arrays for brain-inspired computing,” Nature
507 Materials, vol. 18, pp. 4871–4877, Apr. 2019.
- 508 ⁵⁶ X. Zhang, Y. Zhou, M. Ezawa, G. P. Zhao, and W. Zhao, “Magnetic skyrmion transistor:
509 skyrmion motion in a voltage-gated nanotrack,” Scientific Reports, vol. 5, p. 11369, Sept. 2015.
- 510 ⁵⁷ I.-S. Hong and K.-J. Lee, “Magnetic skyrmion field-effect transistors,” Applied Physics Letters,
511 vol. 115, p. 072406, Aug. 2019.
- 512 ⁵⁸ T. Srivastava, “Mapping different skyrmion phases in double wedges of Ta/FeCoB/TaOx trilay-
513 ers,” Physical Review B, p. 5, 2019.
- 514 ⁵⁹ In reference³⁷, the convention for iDMI sign is opposite to the one used in the present article